Creep of polycrystalline anorthite and diopside

Alexandre Dimanov, Marie-Pierre Lavie, Jannick Ingrin, Georg Dresen, Olivier Jaoul

Creep of polycrystalline anorthite and diopside

A. Dimanov,[1] M. P. Lavie,[2] G. Dresen,[1] J. Ingrin,[2] and O. Jaoul[2]

Received 7 February 2002; revised 31 July 2002; accepted 30 August 2002; published 31 January 2003.

[1] We investigated the creep strength of fine-grained aggregates of single-phase anorthite and diopside at temperatures ranging from 1253 to 1553 K at flow stress between 5 and 250 MPa and at 0.1 MPa pressure. Powders of crushed natural, iron-bearing diopside and of pure anorthite and diopside glasses were hot pressed at temperatures of 1373–1423 K and 300 MPa confining pressure in a gas-medium apparatus and at 1423–1473 K and 2200 MPa in a piston-cylinder device. Grain size of the synthetic materials was 3.4 μm for anorthite and between 1.5 and 7.5 μm for diopside. Creep tests were performed using two uniaxial creep machines in Toulouse and Potsdam. Synthetic anorthite and diopside aggregates showed a stress exponent $n \approx 1$ and a grain size exponent $m \approx -3$, suggesting grain boundary diffusion-controlled creep. Creep rates were independent of oxygen fugacity. Coarser-grained (43 μm) iron-bearing samples showed a transition from diffusion-controlled creep to dislocation creep with $n \approx 5$. Activation energies for diffusion and dislocation creep of iron-bearing diopside polycrystals were $Q = 364–468$ and 719 kJ/mol, respectively. The activation energies for diffusion-controlled creep of synthetic fine-grained anorthite and diopside aggregates were $Q = 362–383$ and 558 kJ/mol, respectively. At similar thermodynamic conditions, diffusion creep rates of diopside are nearly 10 times lower than for anorthite. Irrespective of processing route, the data for anorthite and diopside aggregates from both laboratories are in good agreement. *INDEX TERMS:* 8159 Tectonophysics: Evolution of the Earth: Rheology—crust and lithosphere; 8160 Tectonophysics: Evolution of the Earth: Rheology—general; 3902 Mineral Physics: Creep and deformation; *KEYWORDS:* rheology, anorthite, diopside, creep

Citation: Dimanov, A., M. P. Lavie, G. Dresen, J. Ingrin, and O. Jaoul, Creep of polycrystalline anorthite and diopside, *J. Geophys. Res.*, *108*(B1), 2061, doi:10.1029/2002JB001815, 2003.

1. Introduction

[2] Estimates of lithospheric strength based on laboratory experiments [*Brace and Kohlstedt*, 1984; *Kohlstedt et al.*, 1995] indicate that the lower crust may be substantially weaker than the brittle upper crust and the uppermost mantle. The flow strength of wet quartzite [*Luan and Paterson*, 1992; *Gleason and Tullis*, 1995] is expected to form a lower bound of the strength of the crust below the brittle–ductile transition. Consequently, it has been suggested that a strong upper crust and a strong mantle lithosphere may be "mechanically decoupled." The contribution of the lower crust to the strength of the lithosphere largely depends on the mechanical strength of the dominant mineral constituents, such as feldspar and pyroxene.

[3] Deformation microstructures of natural pyroxene and plagioclase have been investigated extensively (see a review by *Tullis* [1990]). Dislocation creep accompanied by dynamic recrystallization has been demonstrated to be an important deformation mechanism in both minerals [*White*, 1975, 1990; *Olsen and Kohlstedt*, 1985; *Tullis and Yund*, 1985; *Olsen*, 1987; *Skrotzki*, 1994; *Godard and Roermund*, 1995]. However, field studies of exposed sections of the lower crust frequently show highly localized ultramylonite shear zones. In fine-grained (<50 μm) ultramylonites, diffusion-controlled creep may contribute significantly to deformation [*Rutter and Broodie*, 1988; *Kenkmann*, 1997]. In feldspar-bearing and pyroxene-bearing rocks, grain size-sensitive flow is inferred to be an important deformation mechanism accommodating large shear strains >10 [*Boullier and Gueguen*, 1975; *Allison et al.*, 1979; *Jensen and Starkey*, 1985; *White and Mawer*, 1986; *Behrmann and Mainprice*, 1987]. Recently, *Dimanov et al.* [1998, 1999] and *Rybacki and Dresen* [2000] investigated grain size-sensitive creep of polycrystalline plagioclase aggregates. Diffusion creep of diopside aggregates has been recently investigated by *Lavie et al.* [1996], *Lavie* [1998], and *Bystricky and Mackwell* [2001]. However, the effects of grain size and oxygen fugacity on the creep strength of diopside aggregates have not been investigated so far. In this study we present flow laws for diffusion-controlled creep of fine-grained anorthite and diopside aggregates based on an interlaboratory calibration.

[1]GeoForschungsZentrum Potsdam, Potsdam, Germany.
[2]Équipe de Minéralogie, LMTG, UMR 5563, CNRS-Université Paul Sabatier, Toulouse, France.

0148-0227/03/2002JB001815$09.00

2. Experimental Technique

2.1. Sample Preparation

[4] Synthetic anorthite glass powder with an average particle diameter <60 μm (Schott GmbH) contained <1

Table 1. Sample Specifications

Samples	Temp. (K)	Press. (MPa)	Time (h)	Grain Size (μm)	Melt (%)
An01 (anorthite glass < 60 μm)	1423	300	4.5	3.4 ± 3.06	<1
An02 (anorthite glass < 60 μm)	1423	300	4.5	3.4 ± 3.06	<1
An04 (anorthite glass < 60 μm)	1423	300	4.5	3.4 ± 3.06	<1
An05 (anorthite glass < 60 μm)	1423	300	4.5	3.4 ± 3.06	<1
DiGa01 (diopside glass < 60 μm)	1423	300	4.5	7.58 ± 6.21	<2
DiGa02 (diopside glass < 60 μm)	1423	300	4.5	7.58 ± 6.21	<2
DiGb01 (diopside glass < 20 μm)	1373	300	4.5	2.82 ± 1.62	<1
DiGb02 (diopside glass < 20 μm)	1373	300	4.5	2.82 ± 1.62	<1
DiGb03 (diopside glass < 20 μm)	1373	300	4.5	2.82 ± 1.62	<1
DiGc (diopside glass < 20 μm)	1473	2200	96.0	1.51 ± 0.69	0
DiC4 (diopside crystals < 40 μm)	1423	2200	144.0	15.98 ± 8.95	0
DiC6 (diopside crystals < 40 μm)	1423	2200	96.0	15.98 ± 8.95	0
DiC12 (diopside crystals < 40 μm)	1423	2200	96.0	15.98 ± 8.95	0
DiC15 (diopside crystals < 80 μm)	1423	2200	124.0	43.0 ± 33.71	0
DiC18 (diopside crystals < 80 μm)	1423	2200	78.0	43.0 ± 33.71	0

wt.% impurities, mainly Sr, Mn, and Fe. Diopside glass was produced from melting binary oxides with $CaCO_3$ added (Normapur Mercks) in air at 1773–1873 K for 2 hours with subsequent rapid quenching. The impurity content is <1 wt.%. The glass was crushed and ground in alcohol in an agate mortar. We separated particle size fractions of <60 μm (DiGa) and <20 μm (DiGb).

[5] Diopside (DiGa and DiGb) and anorthite (An) aggregates were produced by hot isostatic pressing (HIP) of the powders at 300 MPa confining pressure in a gas-medium apparatus at the GeoForschungsZentrum Potsdam. The powders were first cold pressed in steel jackets with 10 mm diameter and 20 mm length. During HIP, temperature was raised by 20°/min to 1073 K and kept constant for 30 min to fully densify the glass powders. Crystallization of the glass occurred at 1373–1423 K for 4.5 hours. We used Archimedes method and immersion in water or alcohol to estimate the porosities of the resulting An and DiG samples. Porosities were <1%.

[6] To investigate the effects of starting grain size, composition and processing, additional diopside samples were produced in Toulouse using glass powder (DiGc), as well as crystalline powders of iron-bearing diopside obtained from crushed and ground single crystals (DiC). DiC samples were fabricated using powders with a grain size ranging between 20–40 and 60–80 μm, respectively (Table 1). After cold pressing DiGc and DiC samples were jacketed in molybdenum and pure iron containers, respectively, with 4 mm diameter and 8 mm length. Samples were then hot pressed at ≈2200 MPa confining pressure in a piston-cylinder apparatus using cesium chloride as confining medium. The DiGc and DiC samples were hot pressed at 1473 K for 96 hours and 1423 K for 78–144 hours, respectively (Table 1). Porosities of DiGc and DiC samples were estimated by immersion in toluene to be <1% and <1.5%, respectively.

2.2. Microstructures of the Hot-Pressed Specimens

2.2.1. Grain Size and Grain Size Distribution

[7] We determined the grain size of hot-pressed and annealed samples from scanning electron micrographs (SEM) (Figure 1; Zeiss DSM 962; Leo 435VP), and from transmission electron micrographs (TopCon 002B, Philips CM 200 operated at 200 kV equipped with an energy dispersive X-ray (EDX) detector) using the line intercept method [*Underwood*, 1970]. Sample surfaces were broken or polished and chemically or thermally etched. The intercept length distributions of all samples were skewed toward a log-normal shape showing a tail of large grains (Figure 2). The grain size is proportional to the intercept length. Conversion depends on grain shape and aspect ratio. To convert intercept length of anorthite grains into grain size we used a conversion factor of ≈1.9, corresponding to grains with an aspect ratio of ≈2.5 [*Dimanov et al.*, 1998, 1999]. The mean arithmetic grain size of anorthite samples (Figure 1a) was ≈3.40 ± 3.06 μm. The grain size distribution showed a single maximum (Figure 2a). We observed no significant grain growth after >2 days annealing at 1373–1573 K, and the grain size distribution remained unchanged.

[8] Average grain size and grain size distribution of the diopside aggregates varied according to starting material and sintering conditions. The aspect ratio of the grains remained almost equant irrespective of processing route (Figure 1). To convert intercept length into grain size we used a correction factor of 1.776 [*Mendelson*, 1969]. DiGa and DiGb samples displayed a bimodal grain size distribution with a mean of ≈7.58 ± 6.21 μm and a single maximum with a mean of ≈2.82 ± 1.62 μm, respectively (Figures 1b and 1c and 2b and 2c). Grain size and grain size distribution of DiGa samples remained unchanged after annealing. However, the grain size of DiGb samples increased to ≈3.52 ± 1.73 μm after annealing for 3–4 days at temperatures of 1373–1423 K. The starting grain size of DiGc samples was ≈1.53 ± 0.69 μm (Figures 1d and 2d). After annealing at temperatures > 1273 K for 2–3 days, the grain size increased to ≈3.84 ± 1.65 μm and a few grains showed abnormal growth up to 10–15 μm.

[9] Grain crushing and cataclastic flow occurred in all DiC samples hot pressed in the piston-cylinder apparatus resulting in broad, bimodal grain size distributions (Figures 1e and 1f and 2e and 2f). The arithmetic mean grain size was 15.98 ± 8.95 μm (DiC4, DiC6, and DiC12) and 43 ± 33.71 μm (DiC15 and DiC18) for samples fabricated from the 20–40 and 60–80 μm powders, respectively. Grain size and grain size distribution of the DiC samples remained unchanged after annealing for several days.

[10] We define n_i as the number of grains contained in class d_i (with grain size d_i). From each micrograph we

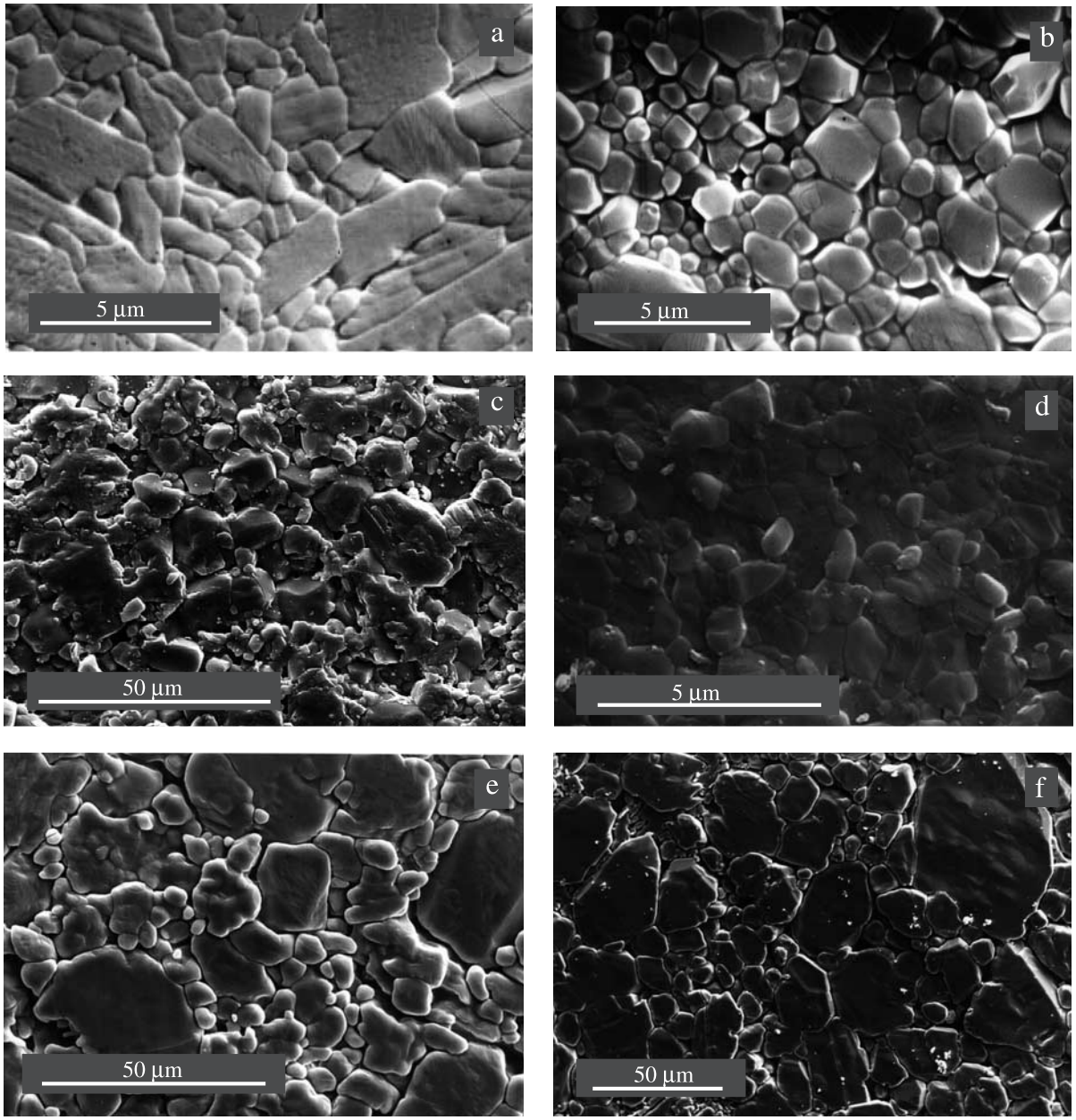

Figure 1. SEM micrographs of hot-pressed starting samples. (a) Thermally etched synthetic anorthite. Grains are prismatic and elongated. Grain size distribution is narrow. (b) Thermally etched synthetic diopside DiGb. Grains are equant, with a narrow grain size distribution. (c) Fractured synthetic diopside DiGa. Grains are equant, with a wide range of grain sizes. (d) Thermally etched synthetic diopside DiGc. Grains are equant. Grain size distribution is narrow. (e) Thermally etched intermediately fine-grained natural diopside DiC (DiC12). Grains are equant. Grain size distribution is wide. (f) Thermally etched coarse-grained natural diopside DiC (DiC18). Grains are equant, with a very wide range of grain sizes.

estimated the area fractions f_i occupied by the n_i grains, that may be expressed as:

$$f_i = \frac{n_i d_i^2}{\sum_i n_i d_i^2} \quad (1)$$

The distributions of area fractions are shown in Figure 2.

2.2.2. Dislocation Density and Twinning

[11] The average dislocation densities of anorthite and diopside samples crystallized from a glass were $<10^{11}$ m^{-2}. The anorthite samples showed many growth twins (Figure 3a) [*Richet et al.*, 1994]. No twins were found in diopside (Figure 3b). Dislocation densities of diopside specimens produced from natural crystal powders (DiC) are higher (up to 10^{13} m^{-2}), but varied significantly between grains. Dislocation walls and twins were frequently found (Figure 3c).

2.2.3. Water Content

[12] Fourier transform infrared (FTIR) spectrometry of the starting glass indicated ≈24 wt ppm H_2O (≈360 H/10^6

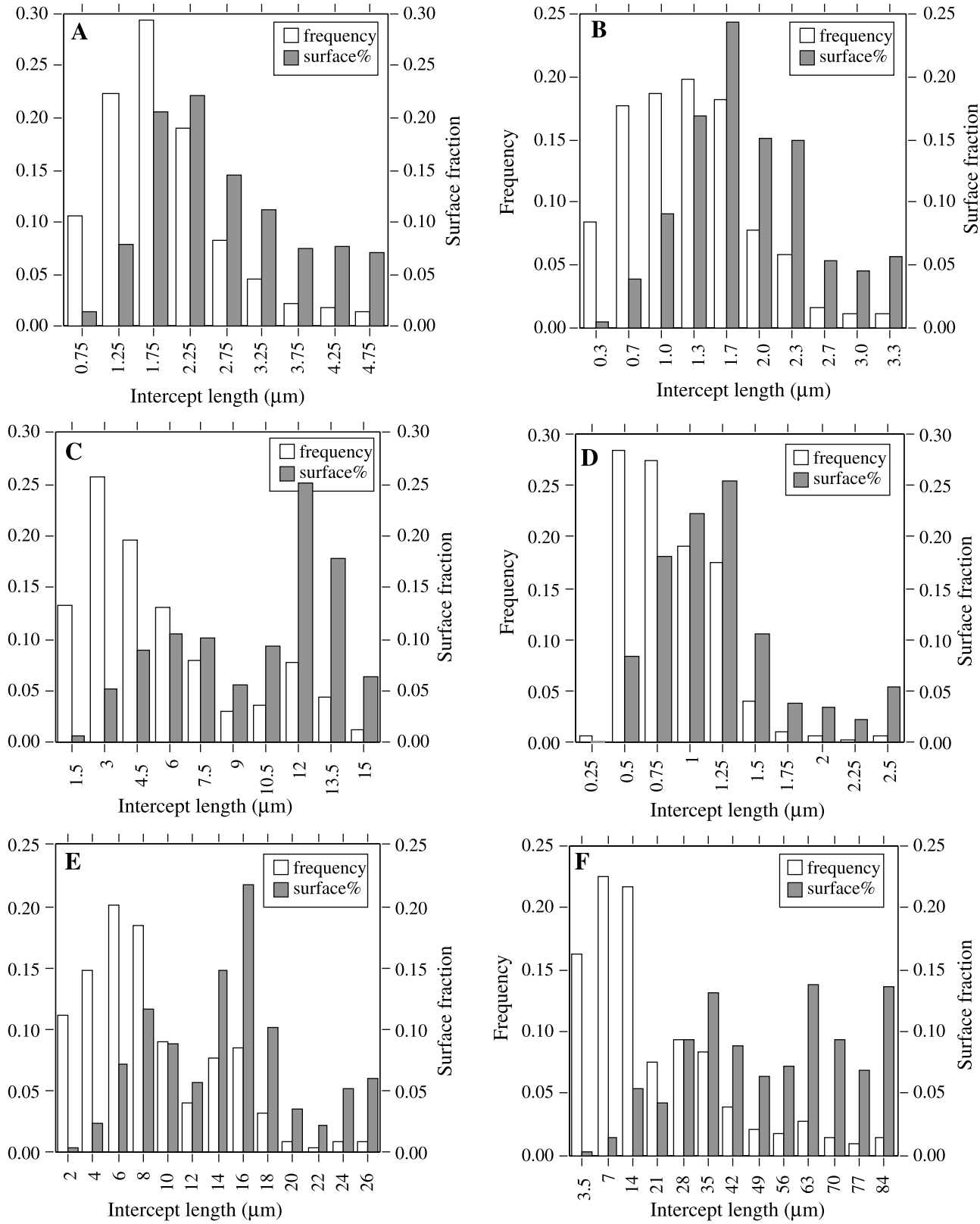

Figure 2. Grain size distributions and the corresponding surface fractions from samples shown in Figure 1. (a). Unimodal distribution in anorthite. (b) Unimodal distribution in samples DiGb. (c) Bimodal distribution in samples DiGa. (d) Unimodal distribution in sample DiGc. (e) Bimodal distribution in sample DiC12. (e) Bimodal distribution in sample DiC18.

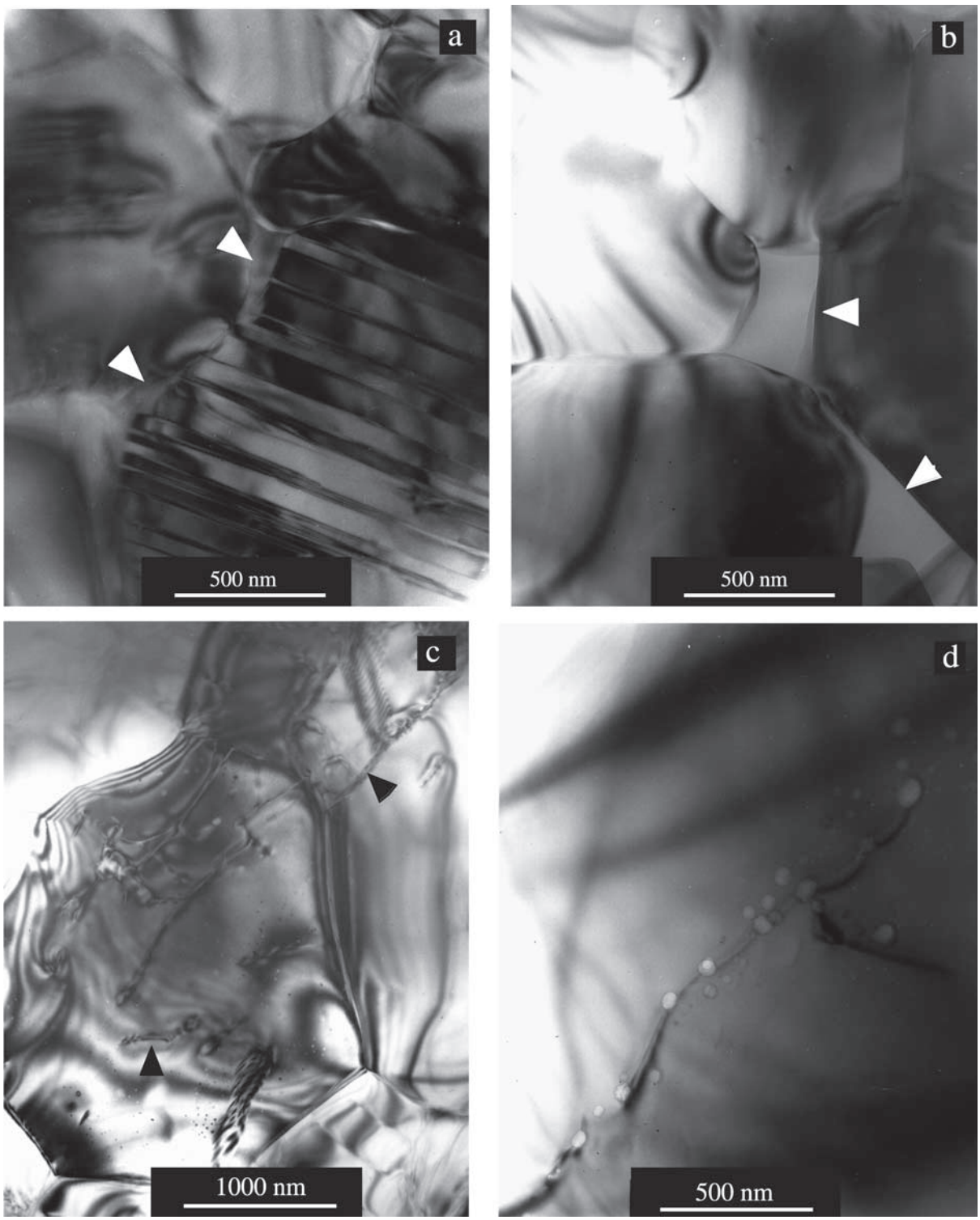

Figure 3. TEM micrographs of hot-pressed samples. (a) Grain triple junctions in synthetic anorthite containing silica-rich melt (arrows). (b) Grain triple junctions in synthetic diopside (DiGa) filled with melt (arrows). (c) Diopside samples DiC contain numerous fluid inclusions. Dislocations (lower arrow) and dislocation walls (upper arrow) are common. No melt is observed. (d) Numerous fluid inclusions are observed in all synthetic materials (here DiGb). In this case, several fluid inclusions are connected to a dislocation.

Table 2. Creep Data for Anorthite Samples

Sample	T (K)	Time (hours)	Log σ (MPa)	Log ε′ (s^{-1})
An04	1393	2.10	0.95	−6.05
	1393	1.60	1.11	−5.81
	1393	1.20	1.37	−5.65
	1393	1.00	1.57	−5.32
	1443	1.05	0.48	−6.05
	1543	0.92	0.30	−5.19
	1543	0.56	0.54	−5.02
	1543	0.48	0.79	−4.75
	1543	0.45	0.96	−4.62
An05	1443	1.00	1.26	−5.02
	1443	1.52	0.98	−5.42
	1443	1.49	1.10	−5.41
	1443	1.04	1.32	−5.12
	1443	1.00	1.60	−4.72
	1443	1.12	1.30	−5.03
	1393	4.13	0.48	−6.45
	1543	0.56	1.11	−4.46
	1543	0.42	1.31	−4.23
	1543	0.38	1.51	−4.01
An01	1323	2.17	0.60	−6.71
	1285	8.07	0.60	−7.11
	1358	2.62	0.60	−6.37
	1378	1.80	0.59	−6.11
	1401	1.23	0.58	−5.88
	1265	8.33	0.58	−7.33
	1393	0.90	0.58	−6.01
	1393	1.33	0.77	−5.80
	1393	0.88	0.89	−5.58
	1393	0.76	0.99	−5.64
	1393	0.66	1.07	−5.57
	1393	0.73	1.14	−5.52
	1393	0.30	1.29	−5.28
	1393	0.38	1.49	−5.01
An02	1265	6.55	0.60	−7.18
	1393	1.70	0.78	−5.66
	1393	0.93	0.90	−5.64
	1393	1.23	1.00	−5.57
	1393	0.67	1.08	−5.55
	1393	0.28	1.20	−5.32
	1393	0.37	1.30	−5.25
	1335	0.67	1.30	−5.98
	1335	8.50	0.78	−6.41
	1335	0.90	1.00	−6.13
	1265	18.50	1.00	−7.29
	1265	13.75	1.15	−6.67
	1265	20.17	1.20	−6.75
	1265	13.58	1.26	−6.58
	1265	4.58	1.38	−6.29
	1265	20.42	1.45	−6.58
	1265	30.50	1.48	−6.53

Si). Water was removed by annealing in air at 1073–1173 K for 2–3 days [*Dresen et al.*, 1996]. Water content of the diopside glass of 16 wt ppm H_2O was estimated using FTIR and the calibration method of *Jendrzejewski et al.* [1996]. Hot-pressed anorthite and diopside samples contained intercrystalline and intracrystalline fluid inclusions (Figure 3d). FTIR spectrometry of the hot-pressed specimens showed a broad absorption band centered at 3400 cm^{-1} indicating the presence of molecular H_2O. After hot pressing the bulk water content of all diopside and anorthite samples was between 250 and 550 wt. ppm H_2O, possibly owing to water adsorbed by the starting glass and crystalline particles. Estimates of the water content of hot-pressed aggregates were based on the calibrations of *Beran* [1986, 1987] for anorthite and of *Bell et al.* [1995] for diopside. Since the samples were fine grained, a large fraction of the water may have been contained in the grain boundaries.

2.2.4. Residual Glass

[13] Anorthite aggregates contained <1 vol.% of silica-rich melt located around fluid inclusions and in three-grain and four-grain junctions (arrows in Figure 3a). A few >1 nm wide melt films could be traced from grain junctions into the grain boundaries. We suggest that the silica-rich melt was formed in contact with the water present in the inclusions [*Dimanov et al.*, 2000]. Migrating grain boundaries may have collected the melt found at three-grain and four-grain junctions. The diopside samples subjected to HIP at 300 MPa contained ≈1–2 vol.% residual glass at three-grain and four-grain junctions (Figure 3b). Some 10–20 nm wide amorphous films decorated a few grain boundaries. Diopside samples subjected to HIP at 2200 MPa (DiC, DiGc) showed no residual glass in TEM observations to a resolution of 1 nm.

2.3. Deformation Experiments

[14] Details of the dead-load deformation apparatuses from Toulouse and Potsdam are given by *Raterron and Jaoul* [1991] and *Dimanov et al.* [1998], respectively. In both machines, a constant load is applied to samples located between alumina pistons and silicon carbide or alumina spacers depending on oxygen fugacity. Friction is minimized using oil seals at the loading pistons. Piston displace-

Table 3. Creep Data for Synthetic Diopside Samples

Sample	T (K)	Time (hours)	Log σ (MPa)	Log ε′ (s^{-1})
DiGa01	1389	61.10	1.53	−7.59
	1389	80.75	1.40	−7.70
	1409	49.74	1.28	−7.50
	1409	24.66	1.61	−7.22
	1409	81.37	1.27	−7.68
	1409	33.57	1.55	−7.28
	1429	12.19	1.55	−6.83
	1429	41.85	1.10	−7.39
	1429	32.45	1.28	−7.29
	1429	26.43	1.27	−7.17
	1429	27.01	1.28	−7.23
DiGa02	1388	121.21	1.30	−7.86
	1369	165.21	1.40	−7.99
	1388	81.98	1.48	−7.69
	1369	119.69	1.40	−7.86
DiGb01	1373	80.05	0.96	−7.47
	1413	42.00	0.96	−7.13
	1433	21.20	0.96	−6.72
DiGb02	1373	33.12	0.85	−7.24
	1373	24.15	1.11	−7.11
	1383	12.62	1.00	−6.99
	1393	9.13	1.06	−6.79
	1393	18.57	0.74	−7.14
	1403	7.05	1.13	−6.61
	1413	5.35	1.11	−6.37
	1423	5.15	0.89	−6.50
	1433	2.86	0.85	−6.23
	1433	1.47	1.11	−5.95
	1433	3.48	0.76	−6.39
	1413	6.24	0.89	−6.62
	1413	4.02	1.22	−6.37
DiGb03	1393	8.92	1.40	−6.72
	1393	30.05	0.97	−7.27
	1373	12.31	1.63	−6.84
DiGc03	1383	47.00	1.46	−6.93
	1383	17.50	1.64	−6.56

Table 4. Creep Data for Natural Diopside Samples

Sample	T (K)	Time (hours)	Log σ (MPa)	Log pO_2 (atm)	Log ε' (s^{-1})
DiC4	1323	180.00	1.80	−16.00	−9.05[a]
	1323	370.00	1.91	−16.00	−9.04
	1323	320.00	2.01	−16.00	−8.98
	1323	140.00	2.08	−16.00	−8.85
	1323	180.00	2.15	−16.00	−8.78
	1348	165.00	2.15	−15.52	−8.51
	1363	140.00	2.15	−15.30	−8.37
	1383	140.00	2.15	−15.10	−8.13
	1403	86.00	2.14	−14.52	−7.91
	1423	72.00	2.14	−14.30	−7.69
	1443	48.00	2.15	−14.16	−7.36
	1463	21.00	2.15	−13.52	−6.98
	1483	24.00	2.15	−13.30	−6.54
	1373	250.00	2.14	−15.16	−8.70
	1393	130.00	2.14	−14.70	−8.32
	1413	53.00	2.14	−14.40	−7.79
	1433	53.00	2.14	−14.22	−7.30
DiC6	1383	295.00	1.49	−15.10	−8.79
	1383	203.00	1.71	−15.10	−8.55
	1383	155.00	1.85	−15.10	−8.41
	1383	135.00	1.96	−15.10	−8.31
	1383	300.00	2.04	−15.10	−8.27
	1383	140.00	2.04	−12.30	−8.33
	1383	165.00	2.04	−11.60	−8.53
	1383	120.00	2.04	−16.40	−8.37
	1383	90.00	2.04	−14.70	−8.4
	1383	62.00	2.04	−12.00	−8.38
	1383	84.00	2.04	−15.89	−8.52
	1383	118.00	2.04	−13.50	−8.34
DiC12	1369	99.00	2.22	−1.68	−8.03
	1379	85.00	2.22	−1.68	−7.98
	1389	69.00	2.22	−1.68	−7.81
	1389	82.00	1.97	−6.00	−7.96
	1389	151.00	1.65	−1.68	−8.26
	1409	48.00	2.22	−1.68	−7.48
	1419	30.00	2.22	−1.68	−7.44
	1429	28.00	2.22	−1.68	−7.28
	1439	20.00	2.22	−1.68	−7.32
	1450	18.00	2.22	−1.68	−7.13
	1450	15.00	2.00	−6.00	−7.31
	1450	19.00	2.07	−1.68	−7.33
	1450	45.00	1.74	−1.68	−7.69
	1379	148.00	2.22	−1.68	−8.29
	1419	58.00	2.22	−1.68	−7.74
	1439	15.00	2.22	−1.68	−7.26
	1450	16.00	2.22	−1.68	−7.22
	1459	9.00	2.22	−1.68	−6.92
DiC15	1373	131.00	1.93	−15.10	−8.2[a]
	1393	62.00	1.93	−14.70	−7.91[a]
	1403	72.00	1.97	−14.52	−7.95
	1403	20.00	2.01	−14.52	−7.95
	1403	22.00	2.05	−14.52	−7.88
	1423	45.00	2.05	−14.30	−7.65[b]
	1423	62.00	2.09	−14.30	−7.69
	1423	64.00	2.12	−14.30	−7.66
	1423	61.00	2.18	−14.30	−7.41
	1423	38.00	2.24	−14.30	−7.16
	1423	104.00	1.91	−14.30	−7.91[c]
	1423	22.00	1.97	−14.30	−7.72[c]
	1423	63.00	2.05	−14.30	−7.48[c]
	1423	52.00	2.09	−14.30	−7.31[c]
DiC18	1403	36.00	2.22	−14.52	−8.03
	1413	88.00	2.22	−14.40	−7.91
	1413	42.00	2.24	−14.40	−7.89
	1413	46.00	2.27	−14.40	−7.86
	1413	68.00	2.29	−14.40	−7.83
	1413	84.00	2.31	−14.40	−7.79
	1413	139.00	2.33	−14.40	−7.65
	1413	45.00	2.37	−14.40	−7.44
	1373	137.00	2.37	−15.10	−8.22
	1393	48.00	2.37	−14.70	−7.75
	1413	60.00	2.02	−14.40	−7.99[c]
	1413	45.00	2.10	−14.40	−7.80[c]
	1413	22.00	2.16	−14.40	−7.65[c]
	1423	21.00	2.14	−14.30	−7.30[c]
	1423	93.00	1.74	−14.30	−8.14[c]
	1423	77.00	1.88	−14.30	−7.90[c]

[a]Steady state was not achieved.
[b]Chart recorder problems.
[c]Records after a short electrical power breakdown.

ment is measured differentially at the sample within 0.5 μm using two linear-variable displacement transducers. Oxygen fugacity is varied using mixtures of CO/CO_2 (Potsdam) and $H_2/H_2O/Ar$ (Toulouse). In Potsdam, cooling circuits in the base plates reduce thermal expansion of the loading frame. Temperature is controlled to within 1 K using Pt/Pt-13%RH or Pt/Pt-10%RH thermocouples located next to the sample. Displacement, temperature, and load are recorded continuously during the experiments.

[15] Tests on anorthite samples were performed at temperatures between 1263 and 1553 K, and axial stresses were between 2 and 32 MPa. For tests on diopside specimens, temperature ranged from 1323 to 1483 K, and axial stresses varied between 5.5 and 235 MPa. In tests on iron-bearing diopside (DiC) samples, oxygen fugacity f_{O_2} was varied between 10^{-11} and 10^{-17} MPa. Sample DiC12 was deformed at $f_{O_2} \sim 10^{-6}$ MPa in argon and at $f_{O_2} \sim 2 \times 10^{-2}$ MPa in air. For the anorthite and diopside samples produced from glass, oxygen fugacity was set to $\sim 10^{-6}$ MPa by argon. Strain rates ε' varied from 1×10^{-4} to $1 \times 10^{-8.5}$ s^{-1} (Potsdam) and $1 \times 10^{-6.5}$ to 1×10^{-10} s^{-1} (Toulouse). Samples were parallelepipeds with dimensions of $\sim 2.5 \times 2.5 \times 5$ mm^3. Creep tests were performed as stress and temperature steps up to 1–2% strain. In most experiments a constant strain rate was reached after <0.5% axial strain. Maximum total strain per specimen was <15%. Constant volume was assumed correcting stress for changes in cross-sectional area. Between the two laboratories, data from individual tests was reproducible within a factor of <2, and different results did not indicate a systematic error.

3. Results

3.1. Mechanical Data

[16] The creep data (Tables 2, 3, and 4) were fit to a power law of the form:

$$\varepsilon' = A p_{O_2}^{p} \sigma^{n} d^{m} \exp(-Q/RT) \quad (2)$$

where ε' is the strain rate in (s^{-1}), A is a constant (s^{-1} $Pa^{-(n+p)}$ m^m), pO_2 is oxygen partial pressure (Pa), σ is stress (Pa), d the grain size in meters, Q is activation energy in kJ/mol, p is oxygen fugacity exponent, n is stress exponent, m is grain size exponent, R and T are universal gas constant and temperature, respectively. Data from Toulouse and Potsdam are shown in Figures 4 and 5 as filled and open symbols, respectively.

[17] At stresses <160 MPa, stress exponents for anorthite and fine-grained (d < 16 μm) diopside aggregates were $n \cong 1$ with n varying between 0.79 ± 0.11 and 1.28 ± 0.13 between different temperatures (Figures 4a–4c). This sug-

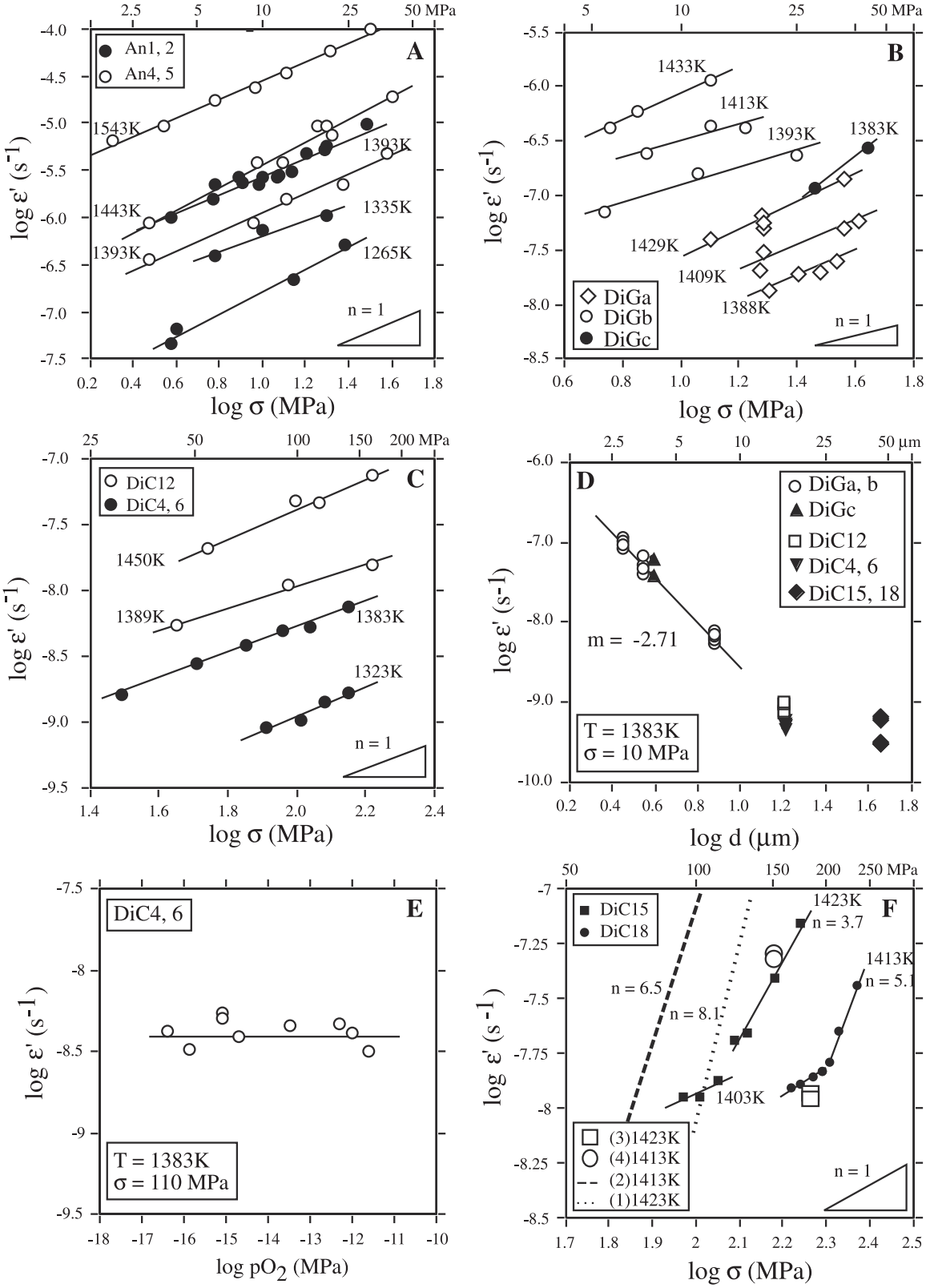

Figure 4. Mechanical data of anorthite and diopside aggregates obtained in Toulouse and Potsdam and plotted as solid and open symbols, respectively. (a) Log stress–log strain rate for anorthite. (b) Log stress–log strain rate for DiG samples. (c) Log stress–log strain rate for fine-grained (d = 16 μm) DiC. (d) Log stress–log average grain size for DiG and DiC samples. (e) Log stress–log pO_2 for DiC samples. (f) Log stress–log strain rate for coarse-grained (d = 43 μm) DiC samples. Data are compared with creep data for single crystals (lines and open symbols) [*Raterron and Jaoul*, 1991; *Raterron*, 1992; *Raterron et al.*, 1994].

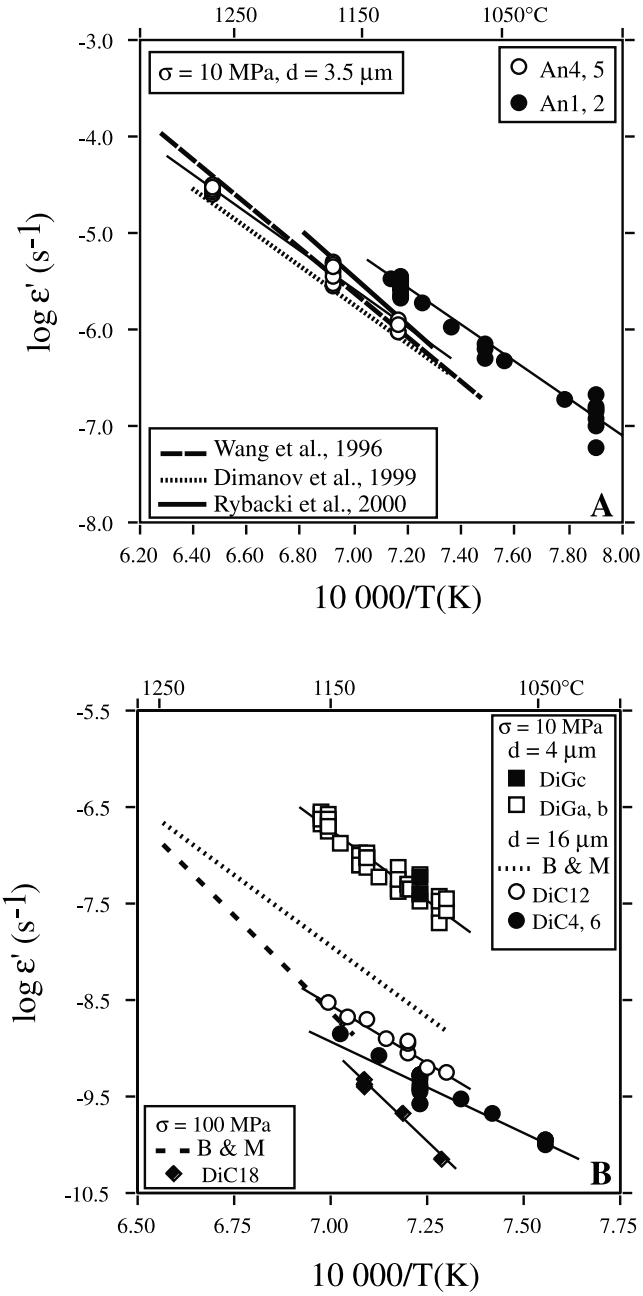

Figure 5. Plot of log strain rate versus inverse temperature with solid and open symbols for data obtained in Toulouse and Potsdam, respectively. (a) Grain boundary diffusion-controlled creep of synthetic anorthite aggregates deformed at atmospheric pressure. The data of *Rybacki and Dresen* [2000] are from experiments performed at 300 MPa confining pressure. (b) Creep of diopside aggregates deformed at atmospheric pressure. The data of *Bystricky and Mackwell* [2000] (B&M) are from experiments performed at 300 MPa confining pressure. The dashed line B&M and the filled diamonds correspond to dislocation creep.

gests that at low stresses deformation of anorthite and fine-grained diopside aggregates was dominated by diffusion-controlled creep. We assume that the observed small differences in the data from tests performed in both laboratories under similar conditions are due to variations in grain size and water content of the specimens introduced during sample preparation. At higher stresses (>160 MPa) coarse-grained diopside samples (DiC15 and DiC18 with d = 43 μm) show a transition from $n \cong 1$ to $n \cong 3-5$, suggesting a transition to dislocation creep (Figure 4f). In the dislocation creep regime the strength of the diopside polycrystals is bounded by the strength of the slip systems operating in diopside single crystals [*Raterron and Jaoul*, 1991; *Raterron*, 1992; *Raterron et al.*, 1994]. At T > 1273 K, slip systems (1−10)[110] and (110)[1−10] are the easiest to activate (Figure 4f, line [2]). No stress exponents have been reported for the strong slip systems ((100)[010], (010)[101], (010)[100] and (100)[001], (010)[001], (110)[001], Figure 4f, open symbols [3] and [4], respectively). However, the strength of our samples showing high stress exponents (n = 3.71 ± 0.48 and n = 5.12 ± 0.54 for DiC15 and DiC18 respectively) is in-between the strengths of single crystals in which the strong slip systems were activated (Figure 4f).

[18] At lower stresses, diopside aggregates deformed by diffusion-controlled creep and creep rates decreased with increasing average grain size. For samples produced from glass, with an average grain size < 8 μm and characterized by either unimodal or slight bimodal grain size distribution (Figures 2b−2d), we found a grain size exponent of $m = -2.7 \pm 0.2$ (Figure 4d). *Dimanov et al.* [1999] estimated a grain size exponent of $m = -2.9 \pm 0.2$ for grain boundary diffusion-controlled creep of pure anorthite aggregates with d < 5 μm. This indicates that at stresses <50 MPa and at temperatures between 1388 and 1433 K, grain boundary diffusion controls the creep rate of fine-grained diopside and anorthite aggregates. However, creep rates of coarse-grained diopside samples with an average grain sizes d = 16 μm (DiC4, DiC6 and DiC12) and d = 43 μm (DiC15 and DiC18), and with pronounced bimodal grain size distributions, did not show a clear dependence on grain size (Figure 4d).

[19] Grain boundary diffusion-controlled creep of Fe-bearing diopside aggregates (d = 16 μm) was not affected by oxygen partial pressure pO_2 (Figure 4e). This is in contrast to dislocation creep of diopside single crystals, containing a similar amount of iron [*Raterron and Jaoul*, 1994].

[20] The activation energies for grain boundary diffusion creep of anorthite aggregates estimated in both laboratories range from 362 ± 29 to 383 ± 21 kJ/mol (Figure 5a), in good agreement with previous studies [*Wang et al.*, 1996; *Dimanov et al.*, 1999]. The activation energies estimated for grain boundary diffusion creep of diopside aggregates are strongly dependent on the starting material. For fine-grained (d < 8 μm) synthetic diopside aggregates (DiG) we find 558 ± 39 kJ/mol. Fe-bearing diopside samples (DiC) with d = 16 μm give activation energies between 468 ± 28 and 364 ± 17 kJ/mol. Dislocation creep of coarse-grained (d = 43 μm) diopside aggregates (DiC18) is characterized by an activation energy of 719 ± 34 kJ/mol, in close agreement with the result of *Bystricky and Mackwell* [2000], who obtained 760 kJ/mol for dry, Fe-bearing diopside deformed at 300 MPa confining pressure. However, the activation energy reported by *Bystricky and Mackwell* [2000] for diffusion creep of dry, Fe-bearing diopside aggregates is substantially

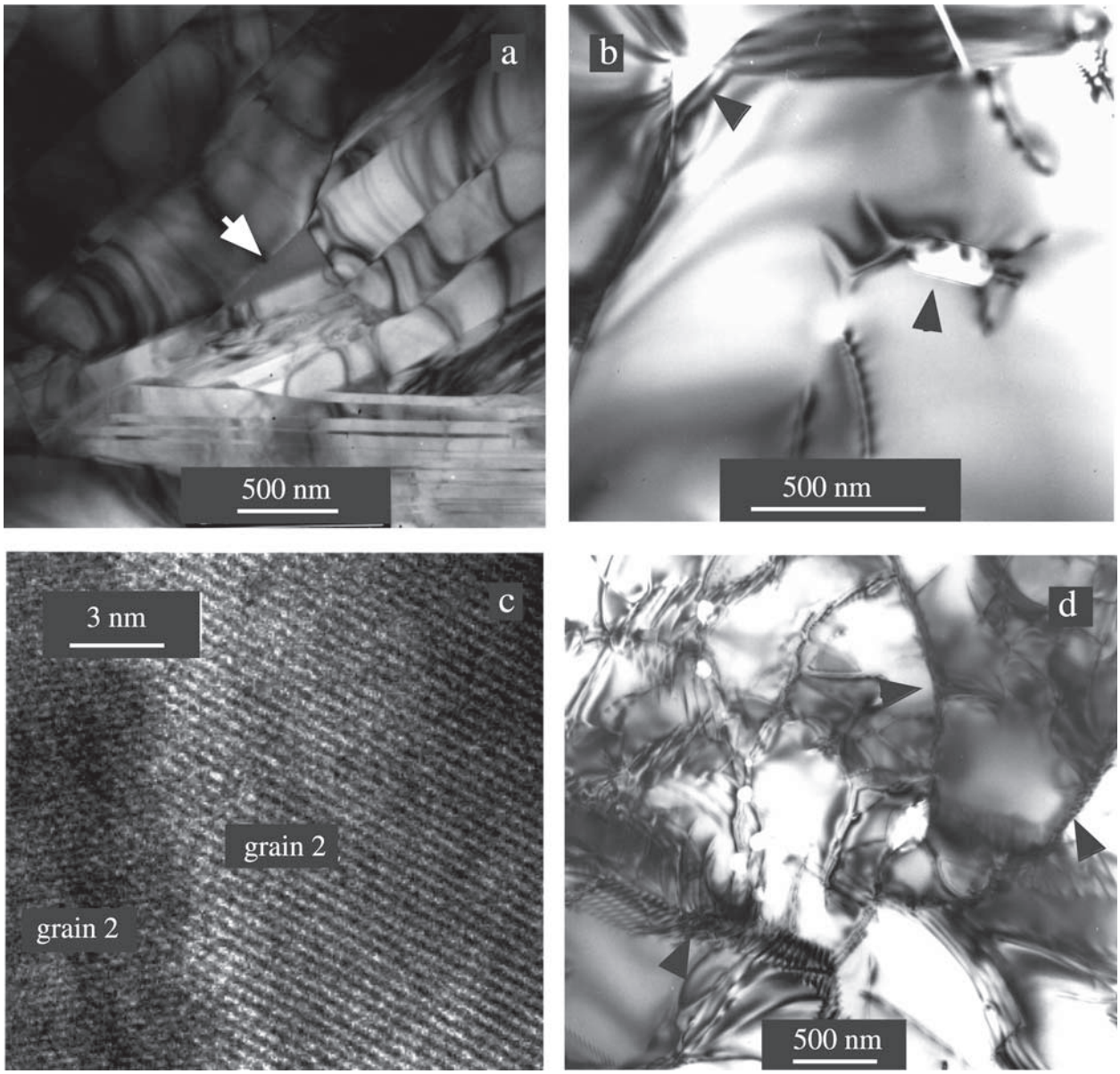

Figure 6. TEM micrographs of deformed specimens. (a) Synthetic anorthite contains some melt-filled triple junctions (arrow), growth twins, but no dislocations. (b) Synthetic diopside shows melt at some grain triple junctions (upper arrow) and a few dislocations, mostly connected to fluid inclusions (lower arrow). (c) Lattice fringes at a grain boundary in synthetic diopside DiGa. The grain boundary is not edge on and grains overlap 2–3 nm. Tilting of the sample shows that there is no amorphous phase at the grain boundary within 1 nm resolution. (d) Coarse-grained (d = 43 μm) DiC18 sample displays numerous free dislocations and subgrains (arrows) indicating recovery.

higher (560 kJ/mol) than in the present study. Possible reasons for this discrepancy will be discussed below.

3.2. Microstructures of the Deformed Specimens

[21] The fine-grained (d < 8 μm) anorthite and diopside samples prepared from glass display low average dislocation densities of $\rho \approx 10^{10}$ to 10^{11} m^{-2} (Figures 6a and 6b). Densities of dislocation and subgrain boundaries in diopside samples prepared from crystalline powder vary substantially. However, in coarse-grained (d = 43 μm) diopside samples (DiC15, DiC18), dislocation densities are as high as $\rho \approx 10^{13}$ m^{-2}, although subgrain boundaries indicating recovery are commonly observed (Figure 6d). The microstructure observed in DiC15 and DiC18 samples indicates a significant contribution of dislocation creep. Deformed diopside samples did not show twinning. In anorthite, density of twins remained unchanged after deformation.

[22] The trace content of melt in diopside and anorthite aggregates hot pressed at 300 MPa from glass was not affected by deformation. For instance, no melt was found on grain boundaries after deformation (Figure 6c) suggesting that melt topology remained unchanged. However, all DiC samples deformed at T > 1423 K show limited partial

Table 5. Flow Law Parameters for Synthetic Anorthite and Diopside Samples

Diffusion-Controlled Creep					
Material	Laboratory	log Ao (m^3 Pa^{-1} S^{-1})	n	m	Q (kJ/mol)
An	Potsdam	−14.941	1	−3	383 ± 21
An	Toulouse	−15.359	1	−3	362 ± 29
DiG	Potsdam	−9.504	1	−3	558 ± 39
DiC	Potsdam	−12.787	1	−3	468 ± 28
DiC	Toulouse	−17.008	1	−3	364 ± 17
Dislocation Creep					
Material	Laboratory	log Ao (m^3 Pa^{-5} S^{-1})	n	m	Q (kJ/mol)
DiC	Toulouse	−22.726[a]	5	nd	719 ± 34

[a]Ao is given for the mean grain size of 45 μm since m was not obtained.

melting resulting in 3–4 vol.% of silica-rich melt. Melt films ~20 nm wide were frequently observed along grain boundaries. Chemically the melt is similar to the partial melt found in diopside single crystals annealed above 1413–1423 K [*Jaoul and Raterron*, 1994]. The mechanical data obtained in the temperature range where partial melting occurred are given in Table 5. However, these data were ignored for the reported flow laws, which are based on data collected below 1423 K only.

4. Discussion

4.1. Grain Size

[23] A stress exponent $n \approx 1$ and a grain size sensitivity of $m = -2.7 \pm 0.2$ (Figures 4b–4d) indicate grain boundary diffusion-controlled creep of fine-grained ($d < 8$ μm) synthetic diopside. The activation energies for Fe-bearing diopside (364–468 kJ/mol) and synthetic diopside samples (558 kJ/mol) are substantially different, suggesting different rate-limiting mechanisms for diffusion-controlled creep.

[24] Coarse-grained samples DiC15 and DiC18 are much weaker than expected from their average grain size (43 μm), when compared to the fine-grained (16 μm) DiC12, DiC4 and DiC6 samples (Figure 4d). These samples display a pronounced bimodal grain size distribution (Figures 2e and 2f). *Bystricky and Mackwell* [2000] deformed diopside aggregates hot pressed from crystalline powders with different narrow ranges of particle sizes (<10, 10–20, and 20–30 μm). Similar to our samples they report particle crushing during cold pressing of the starting diopside powder that resulted in broad grain size distributions. *Bystricky and Mackwell* [2000] did not observe any sensitivity to the average grain size. They suggested that creep rate of the aggregates was rate limited by the diffusion-controlled creep of the small grain size fraction.

[25] Possibly, a contribution of dislocation creep in larger grains obscures the grain size sensitivity of the DiC samples. *Wang* [1994] proposed a constitutive model for combined diffusion and dislocation creep operating in aggregates with unimodal and bimodal grain size distributions. For a bimodal grain size distribution the average grain size is

$$\mathrm{d} = \mathrm{f}_1 d_1 + \mathrm{f}_2 d_2 \tag{3}$$

where d_1 and d_2 are the mean grain sizes of the two modes and f_1 and f_2 the respective fractions. Stresses σ_1 and σ_2 operating on grains d_1 and d_2 result in strain rates ε'_1 and ε'_2. It is assumed that diffusion and power law creep operate in parallel:

$$\varepsilon'_1 = \varepsilon'_{\mathrm{p1}} + \varepsilon'_{\mathrm{d1}}, \tag{4}$$

$$\varepsilon'_2 = \varepsilon'_{\mathrm{p2}} + \varepsilon'_{\mathrm{d2}}, \tag{5}$$

where $\varepsilon'_{\mathrm{p}}$ and $\varepsilon'_{\mathrm{d}}$ refer to power law ($n = n_0$, $m = 0$) and diffusion-controlled creep ($n = 1$, $m = -3$), respectively. The strength of the polycrystalline aggregates is bounded by the isostress and isostrain rate bounds [*Tullis et al.*, 1991]. For an aggregate with a bimodal grain size distribution, assuming uniform stress and concurrent operation of diffusion and dislocation creep, *Wang* [1994] derived a grain size exponent m

$$m = -3\left[\mathrm{f}_1\varepsilon'_{\mathrm{d1}} + \mathrm{f}_2\varepsilon'_{\mathrm{d2}}\right]\left[\varepsilon'_{\mathrm{p}} + \mathrm{f}_1\varepsilon'_{\mathrm{d1}} + \mathrm{f}_2\varepsilon'_{\mathrm{d2}}\right]^{-1} \tag{6}$$

It is clear from (6) that increasing the volume fraction of grains affected by dislocation creep lowers the grain size exponent. However, *Wang* [1994] also showed that the stress exponent is expected to increase while the grain size exponent decreases. This we do not see in our data indicating linear viscous creep ($n \sim 1$).

[26] Here we propose a different approach using an "effective grain size" (d^{eff}) that accounts for strain partitioning between grain size fractions. We assume that grain size fractions d_i of the aggregate are subjected to a uniform stress (uniform stress bound) [*Tullis et al.*, 1991]. Each grain fraction d_i, representing a volume fraction f_i, contributes a volume fraction-weighted strain rate fraction ($\mathrm{f}_i d\varepsilon_i/dt$) to the total sample strain rate ($d\varepsilon/dt$). Using (2), $d\varepsilon/dt$ is expressed by:

$$\frac{d\varepsilon}{dt} = \sum_i \mathrm{f}_i \frac{d\varepsilon_i}{dt} = \sum_i A(\sigma,T)\frac{\mathrm{f}_i}{d_i^3} = A(\sigma,T)\sum_i \frac{\mathrm{f}_i}{d_i^3} \tag{7}$$

In (7) A(σ,T) is a constant depending on stress and temperature. Normalizing the individual strain rate fraction by the total sample strain rate gives a partitioning coefficient S_i:

$$S_i = \frac{(\mathrm{f}_i/d_i^3)}{\sum_i (\mathrm{f}_i/d_i^3)} \tag{8}$$

The effective grain size may then be expressed as:

$$d^{eff} = \sum_i S_i d_i = \sum_i \frac{(\mathrm{f}_i/d_i^3)}{\sum_i (\mathrm{f}_i/d_i^3)} d_i \tag{9}$$

We suggest that the effective grain size better captures the effect of a non-Gaussian grain size distribution on creep than the average grain size. For example, taking the area fractions for classes d_i (Figure 2) as representative of volume fractions f_i, and using (9) for samples DiC18 and DiC12 we obtain effective grain sizes of 21 and 14 μm compared to average grain sizes of 43 and 16 μm, respectively. Clearly, $\mathrm{d}^{\mathrm{eff}}$ is only a rough approximation as is the assumption of a uniform stress distribution in the aggregate. A more elaborated treatment of the grain size

effect on plastic flow was recently presented by *Ter Heege* [2002].

4.2. The Effect of Oxygen Fugacity on Creep of Diopside

[27] *Bystricky and Mackwell* [2000] did not observe an effect of oxygen fugacity on diffusion and dislocation creep rates of Fe-bearing diopside using Fe/FeO and Ni/NiO buffers. However, in deformation tests on Fe-bearing diopside single crystals, *Jaoul and Raterron* [1994] found that dislocation creep rate depends on oxygen fugacity as $d\varepsilon/dt \propto pO_2^{-3/16}$. Also, Ca self-diffusion in Fe-bearing diopside single crystals shows a similar dependence on oxygen fugacity [*Dimanov et al.*, 1996]. Since the single crystals from these studies and the polycrystalline diopside used by *Bystricky and Mackwell* [2000] both contained iron the question arises, if equilibrium with solid buffers was reached in the last study. However, here we show that diffusion-controlled creep rate of Fe-bearing diopside aggregates is independent of oxygen fugacity in the range of 2×10^{-2} to 10^{-17} MPa. This suggests that the type and concentration of point defects dominating transport along grain boundaries may be different from those that dominate volume diffusion. In particular, a high concentration of structure-related ''intrinsic defects'' at the grain boundary may leave oxygen fugacity-dependent changes in the concentration of extrinsic defects undetected.

4.3. Activation Energy

4.3.1. Activation Energy of Anorthite and the Effect of Water

[28] Molecular water is readily adsorbed to the fine-grained powders during processing and cold pressing. Most of it is lost during uniaxial hot pressing and the activation energy for diffusion creep of dry anorthite is $Q = 585 \pm 45$ kJ/mol [*Dimanov et al.*, 1999]. During HIP at 300 MPa of anorthite glass powder adsorbed water is readily incorporated into intracrystalline and intercrystalline fluid inclusions. The fluid inclusions provide a reservoir for water diffusing slowly to the grain boundaries, resulting in lower activation energy ($Q = 377 \pm 38$ kJ/mol) for grain boundary diffusion-controlled creep at 0.1 MPa [*Dimanov et al.*, 1999]. The activation energies for diffusion creep of anorthite estimated in this study ($Q = 362 \pm 29$ to 383 ± 21 kJ/mol) are in good agreement with the results of *Dimanov et al.* [1999]. For samples hot pressed and deformed at 300 MPa confining pressure the activation energy is $Q = 170 \pm 6$ kJ/mol for diffusion-controlled creep [*Rybacki and Dresen*, 2000]. The significant differences in activation energies and creep rates determined from experiments at 0.1–300 MPa point toward the effect of water content and water fugacity on grain boundary diffusion-controlled creep of anorthite.

4.3.2. Activation Energy of Diopside and the Effect of Fe Content

[29] All diopside samples were preannealed at 1373 K in argon, for 2 days prior to deformation. Oxygen fugacity was fixed by the impurity content of the argon at $\approx 10^{-6}$ MPa. Assuming water as the main impurity in the argon (99.99% pure) we estimate a water fugacity $\approx 10^{-3}$ MPa and a hydrogen fugacity $\approx 10^{-6}$ MPa. The activation energy of 558 ± 39 kJ/mol estimated for diffusion creep of the synthetic diopside samples is comparable to the activation energy estimated for dry synthetic anorthite ($Q = 585 \pm 45$ kJ/mol) [*Dimanov et al.*, 1999]. This may indicate that the intrinsic grain boundary diffusivities controlling creep of dry synthetic anorthite and diopside may be related to a similar point defect. However, the activation energy for diffusion creep of dry, Fe-bearing natural diopside aggregates is from 364 ± 17 to 468 ± 28 kJ/mol. The DiC4, DiC6, DiC15 and DiC18 samples were deformed at low hydrogen and water fugacities ($\approx 4 \times 10^{-5}$ to 2×10^{-3} MPa) using different H_2/H_2O/Ar mixtures to control oxygen fugacity. Sample DiC12 was deformed in argon and in air. The diffusion creep rates for all DiC samples are similar, irrespective of oxygen, hydrogen and water fugacities. This suggests that the small differences in thermodynamic conditions in the experiments performed on DiG and DiC samples probably do not account for the observed difference in activation energies. This difference is more likely related to the different impurity content of the natural and synthetic samples. Fe as a major impurity in DiC samples may segregate to the grain boundaries affecting defect formation and/or defect migration of major ionic species. The activation energies for volume diffusion of calcium and oxygen are similar in both synthetic and natural iron-bearing diopside [*Dimanov et al.*, 1996; *Pacaud et al.*, 2001]. However, silicon is known to be the slowest species diffusing in natural diopside [*Bejina and Jaoul*, 1996]. Presumably, Si limits the coupled diffusion process involved in diffusion-controlled creep, but the effect of Fe content on Si diffusion is not known. Likewise, grain boundary diffusion of Si in diopside has not been investigated so far. We can not rule out that other impurities may also influence the activation energy for diffusion-controlled creep. For example, *Bystricky and Mackwell* [2000] obtained a high activation energy (560 ± 30 kJ/mol) for dry diopside aggregates hot pressed from crushed natural polycrystals with compositions different from ours.

4.4. Dislocation Creep of Coarse-Grained Diopside

[30] Coarse-grained samples DiC18 and DiC15 show a transition from diffusion-controlled creep ($n \approx 1$) to dislocation creep ($n > 3$) with increasing and stress (Figure 4f). Dislocation densities observed in the deformed samples increase with increasing stress and frequently observed subgrain boundaries indicate dislocation climb (Figure 6d). The stress exponent and the activation energy estimated for dislocation creep of sample DiC18 at temperatures ranging from 1373 to 1413 K are $n = 5.1 \pm 0.5$ and $Q = 719 \pm 34$ kJ/mol. Flow strength, stress exponent and activation energy determined from polycrystalline diopside DiC18 are very similar to previously published data for diopside single crystals [*Raterron et al.*, 1994] and are in good agreement with data from dry diopside polycrystals deformed in the dislocation creep regime at 300 MPa [*Bystricky and Mackwell*, 2000].

4.5. Melt

[31] The synthetic anorthite and diopside (DiGa and DiGb) samples hot pressed at 300 MPa contain <2 vol.% melt at grain triple junctions. No melt was found at the grain boundaries. Synthetic diopside (DiGc) samples hot pressed at 2200 MPa did not contain melt. However, at the same

conditions we did not find a significant difference in strength between the different types of synthetic diopside samples, suggesting that a small amount of melt restricted to triple junctions does not affect the aggregate strength significantly. This agrees with the findings of *Cooper and Kohlstedt* [1984, 1986] and *Hirth and Kohlstedt* [1995a] for olivine and of *Dimanov et al.* [1998, 2000] for plagioclase. Dimanov et al. observed that a small volume fraction (<5 vol.%) of melt does not strongly enhance the rate of grain boundary diffusion creep, provided the melt does not wet the grain boundaries.

[32] Diopside DiC aggregates produced from crushed natural crystals and deformed at T > 1413–1423 K contain 3–4 vol.% silica-rich melt wetting grain boundaries. In Fe-bearing diopside single crystals *Ingrin et al.* [1991], *Doukhan et al.* [1993], and *Jaoul and Raterron* [1994] observed the formation of microdroplets of silica-rich melt at T > 1413–1423 K. Melt composition and melt content in their samples varied with annealing time. Activation energy for diffusion-controlled creep of diopside aggregates is strongly affected by the presence of melt. Samples deformed at T > 1413–1423 K when melting occurred give an activation energy $Q \approx 600$ kJ/mol as opposed to melt-free samples deformed at lower temperatures. As observed by *Hirth and Kohlstedt* [1995a] for olivine–basalt aggregates, progressive melting with increasing temperature enhances the strain rates resulting in a higher apparent activation energy.

[33] At T > 1423 K partial melting of coarse-grained specimens deforming in dislocation creep reduced the sample strength and the observed stress exponent. The presence of partial melt along grain boundaries may facilitate sliding and relax the von Mises compatibility condition. At 1413 K the strength of sample DiC18 is similar to that of strong diopside slip systems (Figure 4f) and the stress exponent is $n \sim 5$. However, sample DiC15 deformed at 1423 K and containing partial melt showed a stress exponent $n < 4$; it was weaker and comparable to the strength of the intermediate slip systems in diopside. With further experimental duration at 1423 K both DiC15 and DiC18 samples had a similar strength to the easy slip systems in diopside, while the stress exponent was as low as $n \sim 2$. This also suggests some contribution of diffusion-controlled grain boundary sliding to the deformation of the samples. *Hirth and Kohlstedt* [1995b] reported similar observations for olivine–basalt aggregates.

5. Conclusions

[34] At temperatures ranging from 1323 to 1423 K, stresses between 5 and 170 MPa and at atmospheric pressure, fine-grained diopside aggregates showed a stress exponent $n \approx 1$ and a grain size exponent $m \approx -3$. We found that the grain size distribution and the spatial distribution of grains significantly affect the creep behavior of an aggregate. For a bimodal grain size distribution the average arithmetic grain size does not adequately represent the grain size spectrum. From this study and previously published data we found that the diffusion creep rate of pure diopside aggregates is ≈10 times lower than for pure anorthite aggregates at given grain size and thermodynamic conditions.

[35] The creep activation energy of synthetic diopside aggregates is $Q = 558$ kJ/mol. However, the activation energy for Fe-bearing diopside aggregates produced from crushed natural, Fe-bearing crystals is in the range of 364–468 kJ/mol. The difference is likely related to the different impurity contents. We observed no significant difference in creep strength between these samples at experimental conditions, but due to different activation energies, Fe-bearing samples may be considerably weaker at lower temperatures.

[36] Fe-bearing diopside samples showed a transition from diffusion creep to dislocation creep with increasing stress. The dislocation creep flow law is in good agreement with previous data for diopside single crystals deformed at similar conditions. At temperatures exceeding 1423 K limited incongruent melting occurs. With increasing amounts of melt the stress exponent of the samples deformed in the dislocation creep field progressively decreases from 5 to 2, and the samples become weaker. It is suggested that the presence of melt along grain boundaries enhances diffusion transport processes and increases the diffusion creep field at the expense of the dislocation creep field.

[37] Mechanical data for both anorthite and diopside materials obtained in the laboratories of Toulouse and Potsdam are in very good agreement.

[38] **Acknowledgments.** We are grateful to D. Neuville (IPGP) for the preparation of the diopside glass, M. Naumann (GFZ) and M. Belot (Toulouse) for the hot pressing of samples, and S. Gehrmann and K. Paech for the TEM thin section preparation. Very special thanks to R. Wirth for assistance with TEM. Jan Tullis and Mervyn Paterson are warmly acknowledged for their constructive reviews. They definitely helped to clarify and improve this work.

References

Allison, I. R., L. Barnett, and R. Kerrich, Superplastic flow and changes in crystal chemistry of feldspars, *Tectonophysics*, *53*, 41–46, 1979.

Behrmann, J. H., and D. Mainprice, Deformation mechanisms in a high-temperature quartz–feldspar mylonite: Evidence for superplastic flow in the lower continental crust, *Tectonophysics*, *140*, 297–305, 1987.

Bejina, F., and O. Jaoul, Silicon self-diffusion in quartz and diopside measured by nuclear microanalysis method, *Phys. Earth Planet. Inter.*, *97*, 145–162, 1996.

Bell, D. R., P. D. Ihinger, and G. R. Rossman, Quantitative analysis of trace OH in garnet and pyroxenes, *Am. Mineral.*, *80*, 465–474, 1995.

Beran, A., A model of water allocation in alcali feldspar, derived from infrared-spectroscopic investigations, *Phys. Chem. Miner.*, *13*, 306–310, 1986.

Beran, A., OH groups in nominally anhydrous framework structures: An infrared spectroscopic investigation of danburite and labradorite, *Phys. Chem. Miner.*, *14*, 441–445, 1987.

Boullier, A. M., and Y. Gueguen, SP-mylonites: Origin of some mylonites by superplastic flow, *Contrib. Mineral. Petrol.*, *50*, 93–104, 1975.

Brace, W. F., and D. L. Kohlstedt, Limits on lithospheric stress imposed by laboratory experiments, *J. Geophys. Res.*, *89*, 4327–4330, 1984.

Bystricky, M., and S. Mackwell, Creep of dry clinopyroxene aggregates, *J. Geophys. Res.*, *106*, 13,443–13,454, 2001.

Cooper, R. F., and D. L. Kohlstedt, Solution-precipitation enhanced diffusional creep of partially molten olivine–basalt aggregates during hot-pressing, *Tectonophysics*, *107*, 207–233, 1984.

Cooper, R. F., and D. L. Kohlstedt, Rheology and structure of olivine–basalt partial melts, *Tectonophysics*, *91*, 9315–9323, 1986.

Courtial, Ph., Propriétés thermodynamique des silicates fondus et des minéraux au voisinage de la fusion, Ph.D. thesis, 162 pp., Univ. Paris VII, Paris, France, 1993.

Dimanov, A., O. Jaoul, and V. Sautter, Ca self-diffusion in natural diopside single crystals, *Geochim. Cosmochim. Acta*, *60*(21), 4095–4106, 1996.

Dimanov, A., R. Wirth, and G. Dresen, High-temperature creep of partially molten plagioclase aggregates, *J. Geophys. Res.*, *103*, 9651–9664, 1998.

Dimanov, A., X. Xiao, G. Dresen, and R. Wirth, Grain boundary diffusion creep of synthetic anorthite aggregates: The effect of water, *J. Geophys. Res.*, *104*, 10,483–10,497, 1999.

Dimanov, A., R. Wirth, and G. Dresen, The effect of melt distribution on the rheology of plagioclase rocks, *Tectonophysics*, *328*, 307–327, 2000.

Doukhan, N., J.-C. Doukhan, J. Ingrin, O. Jaoul, and P. Raterron, Early partial melting in pyroxenes, *Am. Mineral.*, *78*, 1246–1256, 1993.

Dresen, G., Z. Wang, and Q. Bai, Kinetics of grain growth in anorthite, *Tectonophysics*, *258*, 251–262, 1996.

Gleason, G. C., and J. Tullis, A flow law for dislocation creep of quartz aggregates determined with the molten salt cell, *Tectonophysics*, *247*, 1–23, 1995.

Godard, G., and H. Roermund, Deformation-induced clinopyroxene fabrics from eclogites, *J. Struct. Geol.*, *17*, 1425–1443, 1995.

Hirth, G., and D. L. Kohlstedt, Experimental constraints on the dynamics of the partially molten upper mantle: Deformation in the diffusion creep regime, *J. Geophys. Res.*, *100*, 1981–2001, 1995a.

Hirth, G., and D. L. Kohlstedt, Experimental constraints on the dynamics of the partially molten upper mantle, 2, Deformation in the dislocation creep regime, *J. Geophys. Res.*, *100*, 15,441–15,449, 1995b.

Ingrin, J., N. Doukhan, and J. C. Doukhan, High temperature deformation of diopside single crystals, 2, TEM investigation of the defect microstructures, *J. Geophys. Res.*, *95*, 11,477–11,487, 1991.

Ingrin, J., L. Pacaud, and O. Jaoul, Anisotropy of oxygen diffusion in diopside, *Earth Planet. Sci. Lett.*, *192*, 347–361, 2001.

Jaoul, O., and P. Raterron, High-temperature deformation of diopside crystal, 3, Influence of pO_2 and SiO_2 precipitation, *J. Geophys. Res.*, *99*, 9423–9439, 1994.

Jendrzejewski, N., M. Javoy, and T. Trull, Mesures quantitatives de carbone et d'eau dans les verres basaltiques naturels par spectroscopie infrarouge: Partie II: l'eau, *C. R. Acad. Sci.*, *322*, 735–742, 1996.

Jensen, L. N., and J. Starkey, Plagioclase microfabrics in a ductile shear zone from the Jotun nappe, Norway, *J. Struct. Geol.*, *7*, 527–539, 1985.

Kenkmann, T., Verformungslokalisation in gabbroiden Gesteinen, thesis, GeoForschungsZentrum Potsdam, Potsdam, STR97/12, 1997.

Kohlstedt, D. L., B. Evans, and S. Mackwell, Strength of the lithosphere: Constraints imposed by laboratory experiments, *J. Geophys. Res.*, *100*, 17,587–17,602, 1995.

Lavie, M. P., Déformation expérimentale de diopside polycristallin, Ph.D. thesis, 175 pp., Univ. Paris Sud, Orsay, France, 1998.

Lavie, M. P., J. Ingrin, and O. Jaoul, Experimental plastic deformation of hot-pressed natural diopside polycrystals, *Terra Nova Abstr.*, *8*, 39, 1996.

Lavie, M. P., J. Ingrin, and O. Jaoul, Sintering of diopside in piston cylinder, *Eur. J. Mineral.*, 2000.

Luan, F. C., and M. S. Paterson, Preparation and deformation of synthetic aggregates of quartz, *J. Geophys. Res.*, *97*, 301–320, 1992.

Mendelson, M., Average grain size in polycrystalline ceramics, *Am. Ceram. Soc.*, *52*, 443–446, 1969.

Olsen, G., Plagioclase fabric development in a high-grade shear zone, Jotunheimen, Norway, *Tectonophysics*, *142*, 291–308, 1897.

Olsen, G., and D. L. Kohlstedt, Natural deformation and recrystallization of some intermediate plagioclase feldspars, *Tectonophysics*, *111*, 107–131, 1985.

Raterron, P., Fluage et fusion partielle precoce du diopside monocristallin, thesis, 133 pp., Univ. Paris Sud, Orsay, France, 1992.

Raterron, P., and O. Jaoul, High temperature deformation of diopside single crystal, 1, Mechanical data, *J. Geophys. Res.*, *96*, 14,277–14,286, 1991.

Raterron, P., N. Doukhan, O. Jaoul, and J. C. Doukhan, High temperature deformation of diopside IV: predominance of {110} glide above 1000°C, *Phys. Earth Planet. Inter.*, *82*, 209–222, 1994.

Richet, P., J. Ingrin, B. O. Mysen, Ph. Courtial, and Ph. Gillet, Premelting effects in minerals: An experimental study, *Earth Planet. Sci. Lett.*, *121*, 589–600, 1994.

Rybacki, E., and G. Dresen, Dislocation and diffusion creep of synthetic anorthite aggregates, *J. Geophys. Res.*, *105*, 26,017–26,036, 2000.

Rutter, E., and K. Broodie, The role of tectonic grain size reduction in the rheological stratification of the lithosphere, *Geol. Rundsch.*, *77*, 295–308, 1988.

Skrotzki, W., Defect structure and deformation mechanisms in naturally deformed augite and enstatite, *Tectonophysics*, *229*, 43–68, 1994.

Ter Heege, J. H., Relationship between dynamic recrystallization grain size distribution and rheology, thesis, 141 pp., Univ. Utrecht, Utrecht, 2002.

Tullis, J., Experimental studies of deformation mechanisms and microstructures in quartzo-feldspathic rocks, in *Deformation Processes in Minerals, Ceramics and Rocks*, edited by D. J. Barber and P. G. Meredith, Mineral. Soc. of Great Britain and Ireland, London, 1990.

Tullis, J., and R. Yund, Dynamic recrystallization of feldspar: A mechanism of ductile shear zone formation, *Geology*, *13*, 238–241, 1985.

Tullis, T. E., F. G. Horowitz, and J. Tullis, Flow laws of polyphase aggregates from end-member flow laws, *J. Geophys. Res.*, *96*, 8081–8096, 1991.

Underwood, E. E., *Quantitative Stereology*, 247 pp., Addison-Wesley-Longman, Reading, Mass., 1970.

Wang, J. N., The effect of grain size distribution on the rheological behaviour of polycrystalline materials, *J. Struct. Geol.*, *16*, 961–970, 1994.

Wang, Z. C., G. Dresen, and R. Wirth, Diffusion creep of fine-grained polycrystalline anorthite at high temperature, *Geophys. Res. Lett.*, *23*(22), 3111–3114, 1996.

White, J. C., Albite deformation within a basal ophiolite shear zone, in *Deformation Mechanisms, Rheology and Tectonics, Geol. Soc. Spec. Publ.*, vol. 54, edited by R. J. Knipe and E. H. Rutter, pp. 327–333, 1990.

White, J. C., and C. K. Mawer, Extreme ductility of feldspars from amylonite, Parry Sound, Canada, *J. Struct. Geol.*, *8*, 133–143, 1986.

White, S., Tectonic deformation and recrystallization of oligoclase, *Contrib. Mineral. Petrol.*, *50*, 287–304, 1975.

A. Dimanov and G. Dresen, GeoForschungsZentrum Potsdam, Telegrafenberg, D-424, 14473, Potsdam, Germany. (dima@gfz-potsdam.de)

J. Ingrin, M. P. Lavie, and O. Jaoul, Équipe de Minéralogie, LMTG, UMR 5563, CNRS-Université Paul Sabatier, 39 Allées Jules Guesde, F-31000, Toulouse, France.